PROCEEDINGS OF SCIENCE

$K_L - K_S$ mass difference from Lattice QCD

Jianglei Yu*
Physics Department, Columbia University, New York
E-mail: jy2379@columbia.edu

We will report on the first full calculation of the $K_L - K_S$ mass difference in lattice QCD. The calculation is performed on a 2+1 flavor, domain wall fermion, $24^3 \times 64$ ensemble with a 329 MeV pion mass and a 575 MeV kaon mass. Both double penguin diagrams and disconnected diagrams are included in this calculation. The calculation is made finite through the GIM mechanism by introducing a 949 MeV valence charm quark. While the double penguin diagrams contribute a very small fraction to the mass difference, there is a large cancellation between disconnected diagrams and other types of diagrams. We obtain the mass difference ΔM_K=3.30(34) $\times 10^{-12}$ MeV for these unphysical kinematics.

31st International Symposium on Lattice Field Theory - LATTICE 2013
July 29 - August 3, 2013
Mainz, Germany

*Speaker.

PoS(LATTICE 2013)398

1. Introduction

The kaon mass difference ΔM_K with a value of $3.483(6) \times 10^{-12}$ MeV [1] led to the prediction of charm quark fifty years ago. This extremely small mass difference is believed to arise from K^0-$\overline{K}^0$ mixing via second-order weak interaction. However, because it arises from an amplitude in which strangeness changes by two units, this is a promising quantity to reveal new phenomena which lie outside the standard model. In perturbation theory calculation, the standard model contribution to ΔM_K is separated into short distance and long distance parts. The short distance part receives most contributions from momenta on the order of the charm quark mass. As pointed out in the recent NNLO calculation [2], the NNLO terms are as large as 36% of the leading order (LO) and next-to-leading order (NLO) terms, raising doubts about the convergence of QCD perturbation series at this energy scale. As for the long distance part of ΔM_K, so far there is no result with controlled uncertainty available since it is highly non-perturbative. However, an estimation given by Donoghue *et al.* [3] suggest that there can be sizable long distance contributions.

Lattice QCD provides a first principle method to compute non-perturbative QCD effects in electroweak process. We have proposed a lattice method to compute ΔM_K [4, 5]. Preliminary numerical work [6] have been done for ΔM_K on a 2+1 flavor $16^3 \times 32$ DWF ensemble with a 421 MeV pion mass. We obtained a mass difference ΔM_K which ranges from $6.58(30) \times 10^{-12}$ MeV to $11.89(81) \times 10^{-12}$ MeV for kaon masses varying from 563 MeV to 839 MeV. The preliminary work only included parts of the diagrams, which means it was a non-unitary calculation. In this proceeding, we will report on a full calculation with a lighter pion mass including the effects of disconnected diagrams.

2. Evaluation of ΔM_K

We will briefly summarize the lattice method for evaluating ΔM_K here. More details can be found in [6]. The essential step is to perform a second-order integration of the product of two first-order weak Hamiltonians in a given space-time volume.

$$\mathscr{A} = \frac{1}{2} \sum_{t_2=t_a}^{t_b} \sum_{t_1=t_a}^{t_b} \langle 0|T \left\{ \overline{K^0}(t_f) H_W(t_2) H_W(t_1) \overline{K^0}(t_i) \right\} |0\rangle. \tag{2.1}$$

This integrated correlator is represented schematically in Fig. 1. After inserting a sum over intermediate states and summing explicitly over t_2 and t_1 in the interval $[t_a, t_b]$ one obtains :

$$\mathscr{A} = N_K^2 e^{-M_K(t_f - t_i)} \sum_n \frac{\langle \overline{K}^0 | H_W | n \rangle \langle n | H_W | K^0 \rangle}{M_K - E_n} \left(-T - \frac{1}{M_K - E_n} + \frac{e^{(M_K - E_n)T}}{M_K - E_n} \right). \tag{2.2}$$

Here $T = t_b - t_a + 1$ is the the interaction range. The coefficient of the term which is proportional to T in Eq. (2.2) gives us ΔM_K up to some renormalization factors :

$$\Delta M_K = 2 \sum_n \frac{\langle \overline{K}^0 | H_W | n \rangle \langle n | H_W | K^0 \rangle}{M_K - E_n} \tag{2.3}$$

The exponential terms coming from states $|n\rangle$ with $E_n > M_K$ in Eq. (2.2) are exponentially decreasing as T increases. These terms are negligible for sufficiently large T. There will be exponentially

increasing terms coming from π^0 and vacuum intermediate states. We evaluate the matrix element $\langle\pi^0|H_W|K^0\rangle$ and subtract the π^0 exponentially increasing term explicitly from Eq. (2.2). For the vacuum state, we add a pseudo-scalar density term to the weak Hamiltonian to eliminate the matrix element $\langle 0|H_W + c_s\bar{s}\gamma^5 d|K^0\rangle$. Since the pseudo-scalar density can be written as the divergence of the axial current, the final mass difference will not be changed by adding this term. After the subtraction of exponentially increasing terms, a linear fit at sufficiently large T will give us ΔM_K.

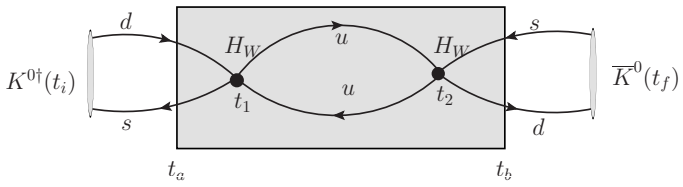

Figure 1: One type of diagram contributing to integrated correlator $\mathscr{A}$. Here t_2 and t_1 are integrated over the time interval $[t_a, t_b]$, represented by the shaded region.

The $\Delta S = 1$ effective Hamiltonian in this calculation is

$$H_W = \frac{G_F}{\sqrt{2}} \sum_{q,q'=u,c} V_{qd} V^*_{q's} (C_1 Q_1^{qq'} + C_2 Q_2^{qq'}) \tag{2.4}$$

where V_{qd} and $V_{q's}$ are Cabibbo-Kobayashi-Maskawa (CKM) matrix elements, C_1 and C_2 are Wilson coefficients for the current-current operators, which are defined as:

$$\begin{aligned} Q_1^{qq'} &= (\bar{s}_i d_i)_L (\bar{q}_j q'_j)_L \\ Q_2^{qq'} &= (\bar{s}_i d_j)_L (\bar{q}_j q'_i)_L \,, \end{aligned} \tag{2.5}$$

The Wilson coefficients are calculated in the $\overline{MS}$ scheme using NLO perpetuation theory [7]. Then the $\overline{MS}$ operators and the lattice operators are connected by using a a Rome-Southampton style style non-perturbative renormalization method [8]. Inserting the weak Hamiltonian into the four point correlators, there will be four type of diagrams as shown in Fig. 2. In our previous work [6], we include only the first two types of diagrams. All the diagrams are included in this work. The type four diagrams, which are disconnected, are expected to be the main source of statistical noise.

3. Details of simulation

This calculation if performed on a lattice ensemble generated with the Iwasaki gauge action and 2+1 flavors of domain wall fermion. The space time volume is $24^3 \times 64$ and the inverse lattice spacing $a^{-1} = 1.729(28)$ GeV. The fifth-dimensional extent is $L_s = 16$ and the residual mass is $m_{res} = 0.00308(4)$ in lattice units. The sea light quark and strange quark masses are $m_l = 0.005$ and $m_s = 0.04$, corresponding to a pion mass $M_\pi = 330$ MeV and a kaon mass $M_K = 575$ MeV. A valence charm quark with mass $m_c^{\overline{MS}}(2\text{ GeV}) = 949$ MeV is used to implement GIM cancellation. We use 800 configurations, each separated by 10 time units.

We will use Fig. 1 to explain the set up of this calculation. We use Coulomb gauge fixed wall sources for the kaons. The two kaons are separated by 31 in lattice unites. The two weak

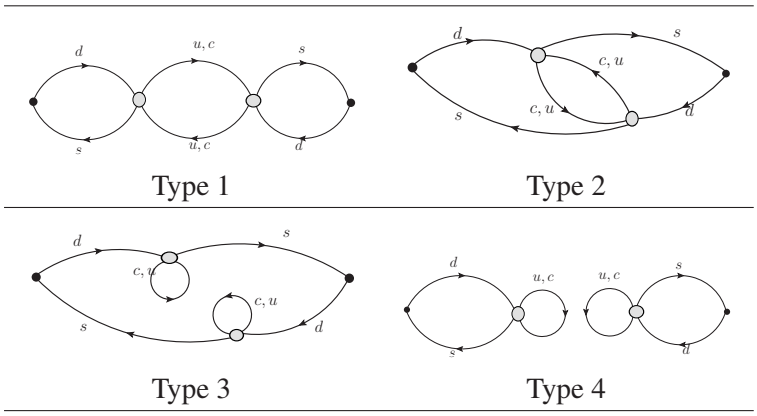

Figure 2: Four type of diagrams contributing the mass difference calculation. The shaded circles represent $\Delta S = 1$ four quark operators. The black dots are γ_5 insertions for kaon sources.

Hamiltonians are at least 6 time slices away from the kaon sources so that the states produced by the kaon interpolating operators are projected onto kaon states. For type 1 and type 2 diagrams, we use the same strategy as in [6]. We compute a point source propagator on each time slice to calculate the quark lines connecting the two weak Hamiltonians. For type 3 and type 4 diagrams, we calculate random wall source propagators to evaluate the quark loops. In order to reduce the noise coming from random numbers, we use 6 sets of random number on each time slice. All the diagrams are averaged over all time translations to increase statistics. For the light quark propagators, which arevthe most expensive part of this calculation, we calculate the lowest 300 eigenvectors of the Dirac operator and use low mode deflation to accelerate the light quark inverters.

4. Fitting results

The results for the integrated correlators are given in Fig. 3(a). The three curves correspond to three different operator combinations: $Q_1 \cdot Q_1$, $Q_1 \cdot Q_2$ and $Q_2 \cdot Q_2$, respectively. The numbers are bare lattice results without any Wilson coefficients or renormalization factors. All the exponential increasing terms have been removed from the correlators. So we expect a linear behavior for large enough T. When T becomes too large, the errors blow up. This is within our expectation since disconnected diagrams have exponentially decreasing signal to noise ratio. The straight lines are the linear fitting results from the data points in the range $[7,20]$. The $\chi^2/d.o.f$ values given in the figure suggest that these fits are robust.

Another method to check the quality of these fits is the effective slope plot, which is an analogy of the effective mass plot. The effective slope at a given time T is calculated using a correlated fit with three data points at $T-1$, T and $T+1$. In Fig. 3(b) we give the effective slope plots for three different operator combinations. The final fitting results and the errors are also given there. For operator combinations $Q_1 \cdot Q_1$ and $Q_2 \cdot Q_2$, we get good plateaus starting from $T = 7$. The result for $Q_1 \cdot Q_2$ is not so satisfying due to large error. However, as we will see later, the $Q_1 \cdot Q_2$ contribution to ΔM_K is very small due to its small lattice amplitudes and its small Wilson coefficients.

We have also tried different fittings to make sure that our results are not sensitive to the parameters we chose. There are two parameters we try to vary: the lower end T_{min} of the time range

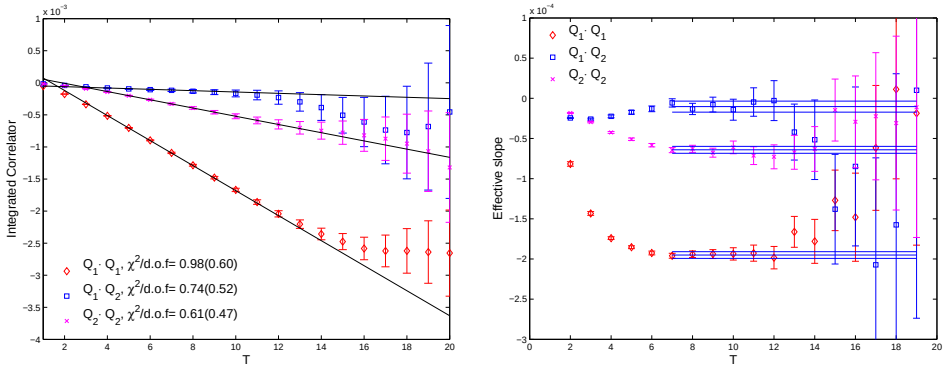

(a) Integrated correlator (b) Effective slope

Figure 3: The left plot gives the integrated correlators for the three operator products $Q_1 \cdot Q_1$, $Q_1 \cdot Q_2$ and $Q_2 \cdot Q_2$. The three lines give the linear fits to the data in the time interval [7,20]. The right plot gives the effective slope plots for three operator products.

of the linear fit and the minimal separation between kaon sources and weak Hamiltonians Δ_{min}. We first fix $\Delta_K = 6$ and vary T_{min} from 7 to 9. The result are given in Table. 1. All the masses are in units of 10^{-12} MeV. While the central value of the fitting results are quite stable, the errors are very sensitive to the choice of T_{min}, which is a feature of disconnected diagrams. In Table. 2, we give the results with fixing $T_{min} = 7$ and ΔM_K from 6 to 8. Both the central values and the errors are very stable, suggesting that a separation of 6 is large enough to suppress the excited kaon states.

Table 1: The fitting results for the mass difference for difference choice of T_{min} while fixing $\Delta_K = 6$. All the masses here are in units of 10^{-12} MeV.

Δ_K	T_{min}	$Q_1 \cdot Q_1$	$Q_1 \cdot Q_2$	$Q_2 \cdot Q_2$	ΔM_K
	7	0.754(42)	-0.16(15)	2.70(18)	3.30(34)
6	8	0.755(45)	-0.10(17)	2.83(23)	3.49(40)
	9	0.758(53)	-0.16(22)	2.69(33)	3.28(55)

Table 2: The fitting results of mass difference for difference choice of Δ_K while fixing $T_{min} = 7$. All the masses here are in units of 10^{-12} MeV.

T_{min}	Δ_K	$Q_1 \cdot Q_1$	$Q_1 \cdot Q_2$	$Q_2 \cdot Q_2$	ΔM_K
	6	0.754(42)	-0.16(15)	2.70(18)	3.30(34)
7	7	0.755(42)	-0.18(15)	2.66(18)	3.23(34)
	8	0.751(42)	-0.18(15)	2.62(19)	3.18(35)

In our previous work, only the first two types of diagrams are included in the calculation. Now that we have the data for all the diagrams, it is interesting to investigate the contribution from type 3 and type 4 diagrams. In Fig. 4, we give the integrated correlators and effective slopes from the combination of type 1 and type 2 diagrams. The results shown in Fig. 5 are from the combination of type 1, 2 and 3 diagrams. In Table. 3, we give the fitting results from difference combination of diagrams. Comparing these results, we can conclude that the contribution from type 3 diagrams is

small and there is a large cancellation between type 4 (disconnected) diagrams and other types of digrams.

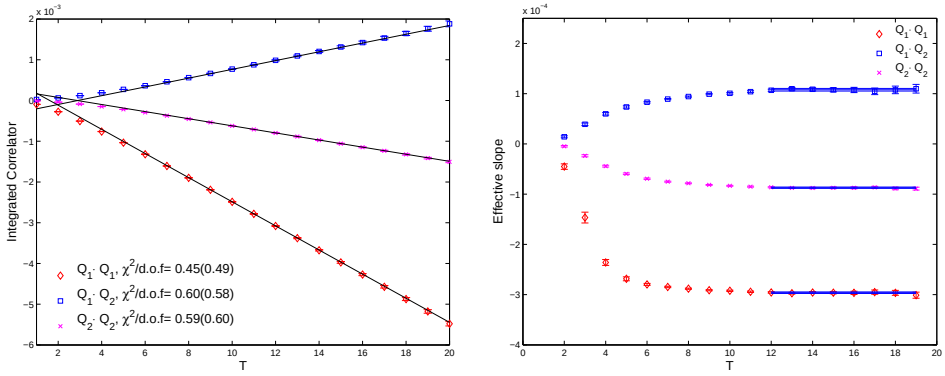

(a) Integrated correlator (b) Effective slope

Figure 4: Results from the combination of type 1 and 2 diagrams. The left plot gives the integrated correlators and the fitting lines. The right plot shows the effective slope.

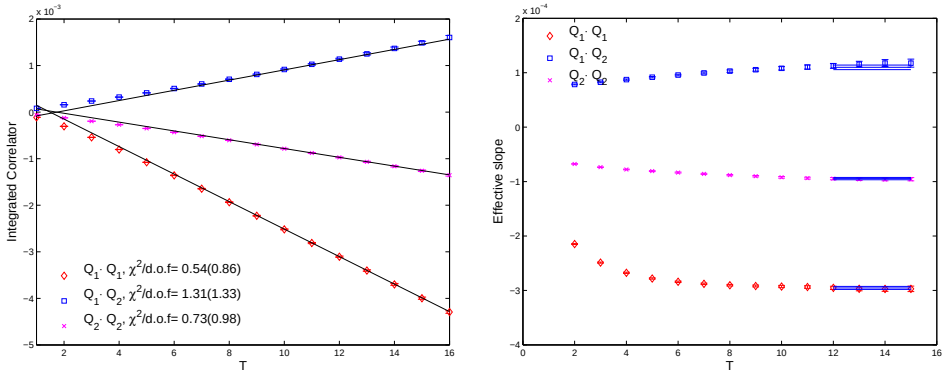

(a) Integrated correlator (b) Effective slope

Figure 5: Results from the combination of type 1, 2 and 3 diagrams. The left plot gives the integrated correlators and the fitting lines. The right plot gives the effective slope plots.

Table 3: Comparison of the mass differences from different combinations of diagrams. All the numbers here are in units of 10^{-12} MeV.

Diagrams	$Q_1 \cdot Q_1$	$Q_1 \cdot Q_2$	$Q_2 \cdot Q_2$	ΔM_K
Type 1,2	1.485(8)	1.567(38)	3.678(56)	6.730(96)
Type 1,2,3	1.481(14)	1.598(61)	3.986(90)	7.07(15)
All	0.754(42)	-0.16(15)	2.70(18)	3.30(34)

5. Conclusions and outlook

We have done a first full lattice calculation of ΔM_K with a 330 MeV pion mass, a 575 MeV

kaon mass and a 949 MeV quenched charm quark mass. Our results is:

$$\Delta M_K = 3.30(34) \times 10^{-12} \quad \text{MeV} \tag{5.1}$$

Only the statistical error is included here. Our result agrees very well with the experimental value $3.483(6) \times 10^{-12}$ MeV. However, since we are not using physical kinematics, this nice agreement maybe fortuitous.

To perform a full calculation with physical kinematics, two difficulties must be overcome. First, we need to perform the calculation on a dynamical four flavor lattice ensemble with a smaller lattice spacing. Thus Thus the effects of charm quenching and the discretization errors coming from the large charm quark mass can be brought under control.. A more challenging problem is the finite volume corrections related with two pions states. This problem will become important if two pion mass is lower than kaon mass. In that case, ΔM_K in continuum limit is given by the principal part of the integral over the two pion momenta, which is quite different from a finite volume sum. A generalization of the Lellouch-Luscher method has been proposed to correct this potentially large finite volume effect [4]. G-parity boundary conditions are required to implement this method [9]. In summary, a full calculation of ΔM_K should be accessible to lattice QCD with controlled systematic errors within a few years.

The author thank very much all his colleagues in the RBC and UKQCD collaborations for valuable discussions and suggestions. Especially thanks to Prof. Norman Christ for detailed instructions and discussions.

References

[1] **Particle Data Group** Collaboration, K. Nakamura *et al.*, *Review of particle physics*, *J.Phys.* **G37** (2010) 075021.

[2] J. Brod and M. Gorbahn, *Next-to-Next-to-Leading-Order Charm-Quark Contribution to the CP Violation Parameter ε_K and ΔM_K*, *Phys.Rev.Lett.* **108** (2012) 121801 [arXiv:1108.2036 [hep-ph]].

[3] J. F. Donoghue, E. Golowich and B. R. Holstein, *LONG DISTANCE CHIRAL CONTRIBUTIONS TO THE K(L) K(S) MASS DIFFERENCE*, *Phys.Lett.* **B135** (1984) 481.

[4] **RBC and UKQCD Collaborations** Collaboration, N. H. Christ, *Computing the long-distance contribution to second order weak amplitudes*, *PoS* **LATTICE2010** (2010) 300.

[5] N. H. Christ, *Computing the long-distance contribution to the kaon mixing parameter ε_K*, *PoS* **LATTICE2011** (2011) 277 [arXiv:1201.2065 [hep-lat]].

[6] N. Christ, T. Izubuchi, C. Sachrajda, A. Soni and J. Yu, *Long distance contribution to the KL-KS mass difference*, arXiv:1212.5931 [hep-lat].

[7] G. Buchalla, A. J. Buras and M. E. Lautenbacher, *Weak decays beyond leading logarithms*, *Rev.Mod.Phys.* **68** (1996) 1125–1144 [arXiv:hep-ph/9512380 [hep-ph]].

[8] G. Martinelli, C. Pittori, C. T. Sachrajda, M. Testa and A. Vladikas, *A General method for nonperturbative renormalization of lattice operators*, *Nucl.Phys.* **B445** (1995) 81–108 [arXiv:hep-lat/9411010 [hep-lat]].

[9] **RBC Collaboration, UKQCD Collaboration** Collaboration, C. Kelly, *Progress towards $\Delta I = 1/2$ $K \to \pi\pi$ decays with G-parity boundary conditions*, *PoS* **LATTICE2012** (2012) 130.